Influence of the nonlinear propagation effect on the optical signal-to-noise ratio of 400G optical fiber communication systems

Huaqiang Qin (秦华强) and Xiaosheng Xiao (肖晓晟)*

State Key Laboratory of Precision Measurement Technology and Instruments, Department of Precision Instrument, Tsinghua University, Beijing 100084, China

**Corresponding author: xsxiao@tsinghua.edu.cn*

Received August 24, 2016; accepted December 23, 2016; posted online February 13, 2017

The influence of the nonlinear propagation effect on three 400 Gb/s/ch (400G) optical fiber communication systems with typical modulation formats, dual-carrier 16-quadrature amplitude modulation (16QAM), single-carrier 16QAM (single-16QAM), and four-carrier quadrature phase-shift keying, are investigated. The received optical signal-to-noise ratio (OSNR), affected by the nonlinear interference noise together with the amplified spontaneous emission noise, are compared with three 400G systems and a standard 100 Gb/s/ch system by numerical simulations. Both single channel and multichannel cases are considered. Single-16QAM is found to have the best OSNR among those modulation formats.

OCIS codes: 060.1660, 060.2330, 190.4370.

doi: 10.3788/COL201715.030604.

Benefitting from complex modulation formats and digital signal processors (DSPs), coherent optical communication has achieved 100 Gb/s/ch (100G) in last a few years, and researchers are working towards 400 Gb/s/ch (400G) in field trials and 1 Tb/s/ch in the laboratory now[1–6]. For 100G systems, the consensus on the modulation format has been reached: polarization-multiplexed quadrature phase-shift keying (PM-QPSK)[7,8]. For 400G systems, there are mainly three methods to achieve that bit rate, and many researchers have done studies about this[9–16]. The first way is to speed up the symbol rate, e.g., achieving 400G signals based on 128.8-GBaud PM-QPSK[10,11]. The second way is to introduce higher-order modulation formats like PM-8\16\32-quadrature amplitude modulation (QAM) and even 64QAM[12–14]. The last way is to increase the subcarrier number of one channel using techniques like orthogonal frequency division multiplexing (OFDM)[15–18]. At present, there is no common standard for the modulation formats of 400G systems. Four-carrier QPSK (four-QPSK), dual-carrier 16QAM (dual-16QAM), and single-carrier 16QAM (single-16QAM)[19–21] are three of the most possible strategies for 400G system in the next generation of commercial optical fiber communication systems. There are a lot of experimental investigations about the performance of 400G systems[10–23]; however, few works think about how noises influence 400G signals, especially, and few works have compared the noises of 400G systems with different modulation formats.

In this Letter, we analyze the influences of nonlinear interference (NLI) noise and amplified spontaneous emission (ASE) noise on the optical signal-to-noise ratio (OSNR) of 400G systems. To figure out how seriously ASE and NLI noises degrade signal quality, we record the data of the OSNRs of the received signals in different cases. We also compare the OSNRs of the single-channel case and the wavelength division multiplexing (WDM) system case. The differences between the signal qualities of a 100G system and three 400G systems are discussed. We point out the advantages of the modulation formats of 400G over that of 100G and which one of the 400G modulation format has the best OSNR in systems affected by ASE and NLI noises.

Table 1 summarizes the modulation formats considered in this Letter, and Fig. 1 shows the abridged general view of two modulation formats of 400G. Figure 1(a) shows dual-16QAM, which has two subcarriers in each channel and a 16QAM constellation diagram of the signal. Figure 1(b) shows four-QPSK, which has four subcarriers in each channel and a QPSK constellation diagram of the signal. The 400G single-16QAM system and 100G system

Table 1. Parameters of Modulation Formats

Bit Rate (Gb/s/ch)	100G	400G	400G	400G
Modulation format	QPSK	Dual-16QAM	Four-QPSK	Single-16QAM
Subcarrier number	1	2	4	1
Channel span (GHz)	50	75	150	75
Symbol rate (Gbaud)	25	25	25	50
Polarization number	2	2	2	2

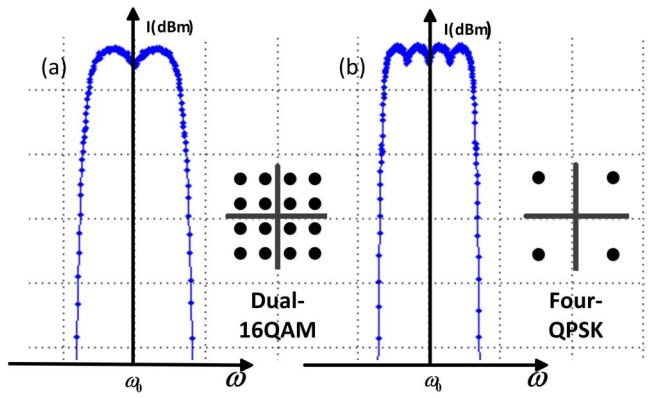

Fig. 1. Spectrum and constellation diagram of 400G with 25 Gsymbol/s. (a) dual-16QAM and (b) four-QPSK.

both have only one subcarrier in each channel. The constellation diagram of the 400G single-16QAM is the same as that in Fig. 1(a), and the constellation diagram of the 100G system is the same as that in Fig. 1(b).

Figure 2 shows the setup of the simulation. 2^{10}–1 pseudo-random binary codes are generated, which drive a Mach–Zehnder modulator to obtain the input optical signal. The parameters of the transmission fiber are listed in Table 2. An erbium-doped fiber amplifier (EDFA) is used to fully compensate the power loss of the signal at the end of each fiber span, inducing ASE noise at the same time. The split-step Fourier method is used to simulate the fiber links. The OSNR is calculated according to the differential resolution bandwidth discrimination approach[24]. The NLI in our simulations only considers the nonlinear optical Kerr effect, including self-phase modulation (SPM), cross-phase modulation (XPM), and four-wave mixing (FWM).

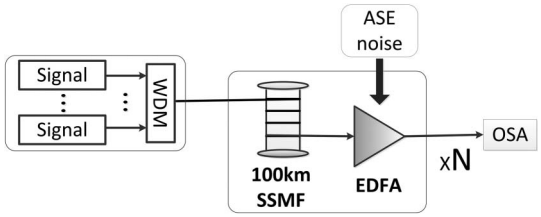

Fig. 2. Setup of simulation. SSMF: standard single-mode fiber, OSA: optical spectrum analyzer.

Table 2. Fiber Parameters

Span length (km)	100
Nonlinear index coefficient	2.6×10^{-20}
Core area (m^2)	80×10^{-10}
Loss (dB/km)	0.2
D (ps/(nm · km))	17

In the simulation of the transmitter, unless otherwise specified, for all four systems, the direct output powers of each laser before modulation (we call it the input channel power in the following text) are the same, no matter how many subcarriers there are. We note that the same input channel power does not imply the same average signal power in the fibers because the modulation losses are different for different modulation formats. For example, the modulation loss of 16QAM is slightly larger than that of QPSK because there is amplitude modulation in 16QAM.

We compare the performances of the 100G system and three 400G systems with a single channel. Figure 3 shows how the signal OSNR changes along with the input power after signal propagates for 5 fiber spans. For a system with a single channel, when the input power is so low the ASE noise is much larger than the NLI noise, the OSNRs of the four systems are linearly proportional to the input powers. In addition, we find the single-16QAM system is better than the dual-16QAM system and 100G is better than four-QPSK. Under the influence of ASE noise, more subcarriers mean a worse OSNR, because the input power is the sum of all the subcarriers' powers.

When the input power is high enough, the OSNRs of all the systems decrease with the increase of the input power due to the NLI noise. Single-16QAM is the best, while 100G is the worst one among the four systems. For the single-channel case, 100G is the most easily affected by NLI noise, and it has the fastest drop speed of the OSNR as the input power increases. The subcarrier and constellation diagram will lower the signal power, so the SPM decreases, but the subcarrier will increase the XPM and FWM. So single-16QAM has the best OSNR due to the lower signal power for the constellation diagram, and there are no XPM and FWM effects among the subcarriers. It is the last one whose signal OSNR starts to decrease, and it shows the best OSNR. Dual-16QAM, similar to four-QPSK, is not the best, but it is not the worst.

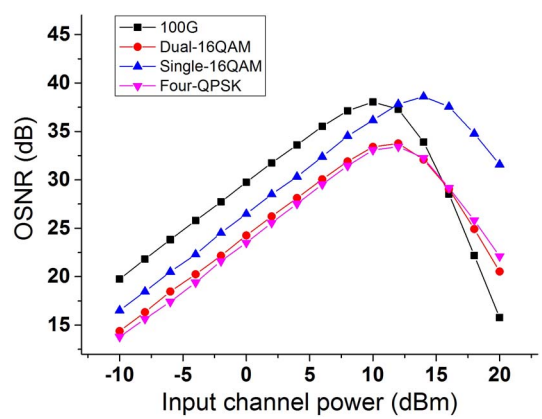

Fig. 3. Signal OSNR versus input power of the 100G single channel system and the three 400G single-channel systems, considering both ASE and NLI noises in uncompensated links with 5 fiber spans.

In later sections, WDM systems are considered. In the simulations, all systems keep the same bit rate at 1.2 Tb/s. There are three channels for 400G systems and twelve channels for 100G system, and all the systems' channel powers are same. Figure 4 plots signal the OSNRs after 5 fiber spans of the 100G system and three 400G systems under the effects of different noise.

Figure 4(a) shows the trend of the signal OSNR versus the input channel power, where only ASE noise affects the signal quality. The conclusions draw from this figure are the same as in the case of the single channel with low input power.

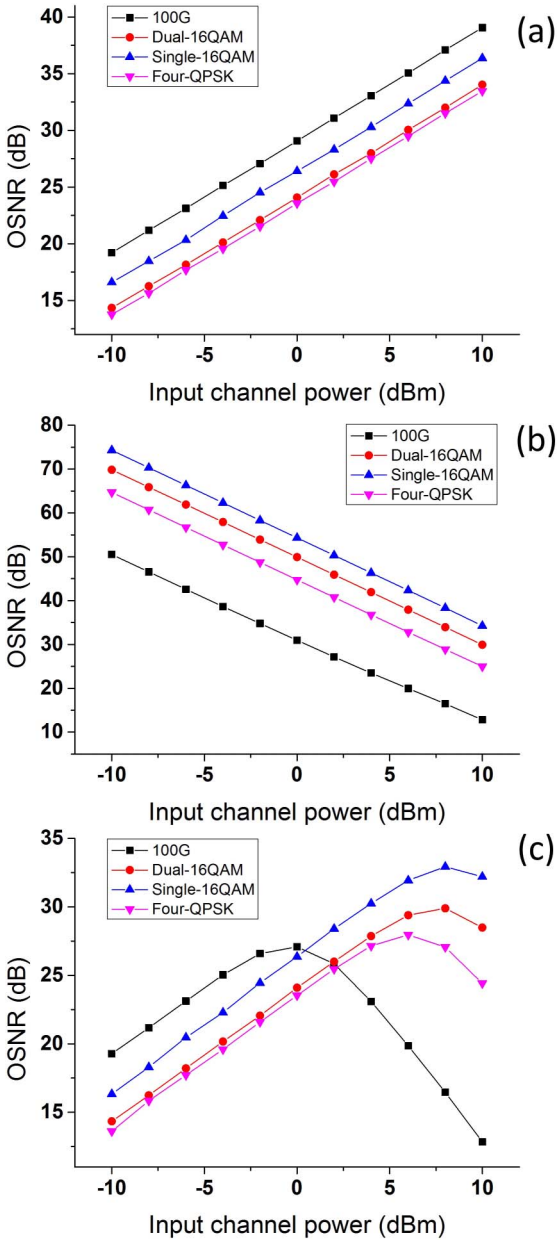

Fig. 4. Signal OSNRs of the 100G system and the three 400G systems with different noises considered. (a) ASE noise only, (b) NLI noise only, and (c) both ASE and NLI noises. The total bit rates are 1.2 Tb/s for all four systems.

When only NLI noise is considered, the trend of the signal OSNR versus the input channel power is shown in Fig. 4(b). From this figure, it is also apparent that the OSNR is inversely proportional to the input power and the slope is −2, since the power of the NLI noise is the cube of the input power. The 100G system has the worst signal OSNR, as shown in Fig. 4(b). Among 400G systems, four-QPSK is the worst, dual-16QAM is better than four-QPSK, and single-16QAM is the best. This can be explained by the following reason: more subcarriers result in more serious XPM and FWM. Besides, the signal power after the modulation of QPSK is slightly higher than that of 16QAM. Therefore, four-QPSK is the worst in these 400G systems, while single-16QAM is the best.

The case with both ASE and NLI noises is plotted in Fig. 4(c). Under the actions of ASE and NLI noises, single-16QAM keeps the best signal quality in the 400G systems, followed by dual-16QAM; four-QPSK is the worst. With the increase of the input power, the OSNRs of all 400G systems increase at first but then decrease after reaching a threshold power. As mentioned before, when the ASE noise dominating the NLI noise, we can say the 100G system and single-16QAM perform better than the others because of their single-subcarrier modulation format. However, when they face NLI noise, things change. The 100G system is the worst one due to its large number of channels, which it needs to achieve the same bit rate as the 400G systems, while single-16QAM is still the best performer. This proves single-16QAM has the lowest NLI noise power.

Compared with the single-channel case, all threshold powers (the powers where the curves change their directions) decrease when there are multiple channels. In the single-channel case (Fig. 3), the OSNR of dual-16QAM is lower than that of four-QPSK at a high input power, and this means the NLI noise in dual-16QAM is more serious. However, in the WDM case [Figs. 4(b) and 4(c)], we find that the effect of the NLI noise on four-QPSK is larger than that on dual-16QAM, which is opposite to the single-channel case. This can be interpreted as follows: the SPM is the main NLI effect in the single-channel case, but XPM and FWM are the main NLI effects in the WDM system.

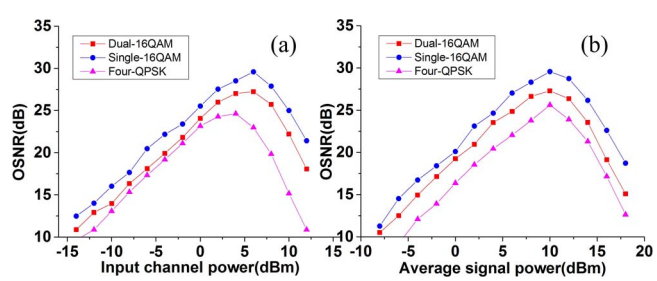

Fig. 5. Signal OSNR of 400G systems with the ASE and NLI noises versus (a) the input channel power and (b) the average signal power in the fiber. The total bit rates are 2.4 Tb/s for all three systems.

To confirm the conclusions above for 400G systems, systems with more WDM channels are compared, as shown in Fig. 5(a). Moreover, 400G systems with the same average signal power in the fiber, instead of the input channel power, are compared in Fig. 5(b). From Fig. 5(a), one can find that these curves have the same trend as those of the 3-channel 400G systems shown in Fig. 4(c). The curves in Fig. 5(b) also have the similar trend as those in Fig. 5(a). Therefore, from Fig. 5, we can draw the same conclusions as those from Fig. 4.

If a system achieves its best signal OSNR at a threshold input power [Fig. 4(c)], this threshold power is referred to as the optimal input power here. Figure 6 shows how the OSNR changes along with the fiber spans under the effects of both ASE and NLI noises in uncompensated links, with the optimal input power of each system obtained from Fig. 4(c). From Fig. 6, we can see the maximum reachable distance of each system at a specific OSNR limitation. For the same OSNR limitation, the signal of single-16QAM can propagate the longest distance in those WDM systems, followed by dual-16QAM, four-QPSK, and 100G, in that order. It should be noted that for a demanded bit error rate (BER), the requirements for the receiver OSNR (OSNR margin) are different for those modulation formats. This OSNR margin is determined by the relation between the BER and the OSNR, which can be evaluated roughly by the formula derived in Refs. [25,26]. In general, single-16QAM has the highest OSNR margin, followed by dual-16QAM, four-QPSK, and 100G. So, when considering the same BER limitation, the conclusion for the maximum reachable distances may vary.

In the simulations above, the input channel powers are kept the same for all four systems, no matter how many subcarriers there are. Here we consider another case, where the subcarrier powers are same for all modulation formats. Figure 7 shows the trend of the signal OSNR after 5 fiber spans versus the input subcarrier powers, which are kept the same for all systems. Just like the trend in

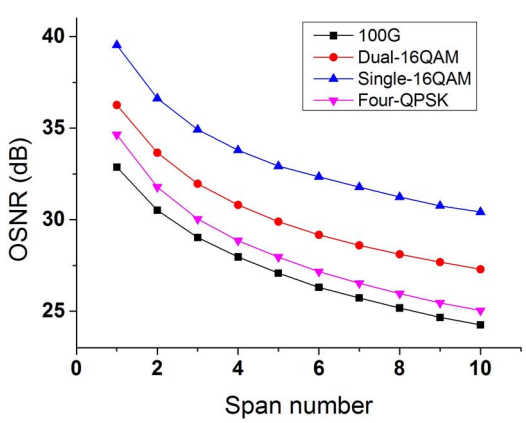

Fig. 6. Signal OSNRs versus the fiber span number of the 100G system and the three 400G systems with both ASE and NLI noises in uncompensated links. The input power of each system is optimized to get the maximum OSNR [as shown in Fig. 4(c)]. The total bit rates are 1.2 Tb/s for all four systems.

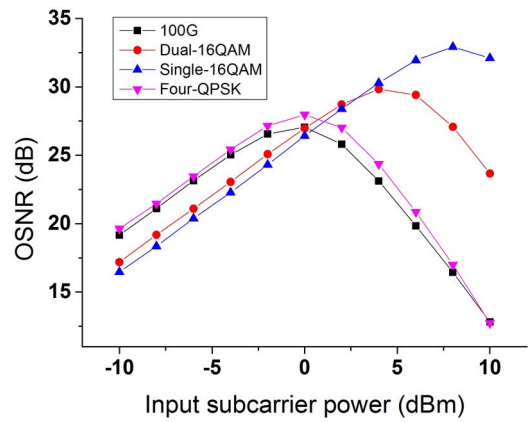

Fig. 7. Signal OSNRs of the 100G system and the three 400G systems versus the subcarrier power. The total bit rates are 1.2 Tb/s for all four systems.

Fig. 4(c), with the increase of power, the OSNR of each system increases at first and then decreases after a threshold power. For single-subcarrier formats (single-16QAM and 100G), the data in Fig. 7 are the same as those in Fig. 4(c). For the multicarrier modulation formats (four-QPSK and dual-16QAM), the channel power is higher; thus, the OSNRs of the two formats in Fig. 7 increase about 3 and 6 dB higher than the OSNRs in Fig. 4(c), respectively, when the power is low. Also, no matter how many subcarriers there are, the signal power in the spectral domain is same for the formats with the same constellation diagram. So in the low input power area in Fig. 7, we can see the coincidence of the OSNRs for the formats with the same constellation modulation. But what we need to worry about is that the multisubcarrier in this case means a higher total power, which would lead to a more serious NLI effect, and so we find that both dual-16QAM and four-QPSK start to decrease the OSNR earlier when compared with Fig 4(c).

In conclusion, the influences of NLI and ASE noises on the received OSNRs of a 100G system and three 400G systems with typical modulation formats are investigated and compared. We find that 100G has the best OSNR with the effect of ASE noise only, while dual-16QAM and four-QPSK are the worst. When considering the effect of NLI noise, single-16QAM has the best OSNR among all the three 400G modulation formats. Under the conditions of the same bit rate and input channel power, 100G is the worst. For the single-channel case and the WDM case, the results are different when compared with the OSNRs of dual-16QAM and four-QPSK. We attribute this to the fact that the main NLI noise for dual-16QAM and four-QPSK is SPM in the single-channel case, but in the WDM systems, XPM and FWM become important. Furthermore, we conclude that single-16QAM does better than the others, followed by dual-16QAM, then four-QPSK, and 100G at the same OSNR limitation and total bit rate on the maximum reachable distance with the effects of ASE and NLI noises for the WDM system case. More simulations with different system parameters give

similar conclusions. It should be noted that the overall performances of coherent communication systems with different modulation formats depends on not only the magnitude of the noise, but other factors, e.g., the endurance of the modulation formats when exposed to noise, and the OSNR margin for a specific BER. More investigations about modulation formats for 400G are required in the future.

This work was supported by the National Key Scientific Instrument and Equipment Development Project of China under Grant No. 2014YQ510403.

References

1. W. Idler, F. Buchali, and K. Schuh, in *Optical Fiber Communication Conference* (2016), Tu3A.7.
2. S. J. Trowbridge, in *Optical Fiber Communications Conference and Exhibition (OFC)* (2015), p. 1.
3. M. Camera, B.-E. Olsson, and G. Bruno, in *36th European Conference and Exhibition on Optical Communication* (2010).
4. C. Gui and J. Wang, Photon. Res. **4**, 168 (2016).
5. Z. He, W. Liu, B. Shen, X. Chen, X. Gao, S. Shi, Q. Zhang, D. Shang, Y. Ji, and Y. Liu, Chin. Opt. Lett. **14**, 040602 (2016).
6. L. Cheng, L. Xi, D. Zhao, X. Tang, W. Zhang, and X. Zhang, Chin. Opt. Lett. **13**, 100604 (2015).
7. P. Dong, J. Lee, Y.-K. Chen, L. L. Buhl, S. Chandrasekhar, J. H. Sinsky, and K. Kim, J. Lightwave Technol. **34**, 79 (2016).
8. R. Younce, J. Larikova, and Y. Wang, in *Asia Communications and Photonics Conference* (2012), AS3A.4.
9. K. Wang, Y. Lu, and L. Liu, in *Optical Fiber Communication Conference* (2015), W3E.2.
10. J. Zhang, J. Yu, B. Zhu, F. Li, H.-C. Chien, Z. Jia, Y. Cai, X. Li, X. Xiao, and Y. Fang, Opt. Express **23**, 16540 (2015).
11. Y. R. Zhou, K. Smith, P. Weir, J. Chen, W. Pan, N. Zhou, and Z. Xiao, in *Optical Fiber Communication Conference* (2016), W3B.3.
12. Z. Jia, H.-C. Chien, J. Zhang, Y. Cai, and J. Yu, in *IEEE Photonics Conference (IPC)* (2015), p. 413.
13. X. Zhou, L. Nelson, R. Issac, P. Magill, B. Zhu, and D. Peckham, in *Optical Fiber Communication Conference* (2012), OM2A.2.
14. Z. Jia, in *Optical Fiber Communication Conference* (2016), Tu3A.4.
15. J. H. Ke, Y. Gao, and J. C. Cartledge, Opt. Express **22**, 71 (2014).
16. F. Li, J. Yu, Z. Cao, M. Chen, J. Zhang, and X. Li, Opt. Express **24**, 2648 (2016).
17. A. H. Gnauck, P. J. Winzer, S. Chandrasekhar, X. Liu, B. Zhu, and D. W. Peckham, in *National Fiber Optic Engineers Conference* (2010), PDPB8.
18. X. Zhou, L. E. Nelson, P. Magill, R. Isaac, B. Zhu, D. W. Peckham, P. I. Borel, and K. Carlson, J. Lightwave Technol. **30**, 553 (2012).
19. Y.-K. Huang, S. Zhang, E. Ip, T. Wang, Y. Aono, and T. Tajima, in *19th Optoelectronics and Communications Conference (OECC) and the 39th Australian Conference on Optical Fibre Technology (ACOFT)* (2014), p. 368.
20. M.-F. Huang, S. Zhang, K. Mino, and Y. Aono, in *Optical Fiber Communication Conference* (2014), Th4F.3.
21. R. Younce, J. Larikova, and Y. Wang, J. Opt. Commun. Networking **5**, A267 (2013).
22. T. J. Xia, G. A. Wellbrock, M.-F. Huang, S. Zhang, Y.-K. Huang, D.-I. Chang, S. Burtsev, W. Pelouch, E. Zak, and W. Szeto, in *Optical Fiber Communication Conference* (2014), Tu2B.1.
23. Y.-K. Huang, D. Qian, F. Yaman, T. Wang, E. Mateo, T. Inoue, Y. Inada, Y. Toyota, T. Ogata, and M. Sato, in *National Fiber Optic Engineers Conference* (2013), NW4E.1.
24. D. Gariepy, G. He, and Y. Breton, "Method and System for Determining in-Band Optical Noise," US Patent 8787753 (2014).
25. R. Schmogrow, B. Nebendahl, M. Winter, A. Josten, D. Hillerkuss, S. Koenig, J. Meyer, M. Dreschmann, M. Huebner, and C. Koos, IEEE Photon. Technol. Lett. **24**, 61 (2012).
26. A. Carena, V. Curri, G. Bosco, P. Poggiolini, and F. Forghieri, J. Lightwave Technol. **30**, 1524 (2012).